Author's Accepted Manuscript

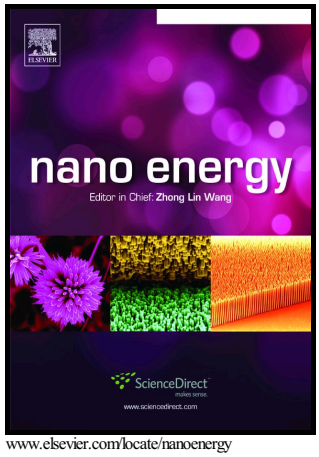

www.elsevier.com/locate/nanoenergy

Piezotronic Effect on Interfacial Charge Modulation in Mixed-dimensional Van der Waals Heterostructure for Ultrasensitive Flexible Photodetectors

Junli Du, Qingliang Liao, Mengyu Hong, Baishan Liu, Xiankun Zhang, Huihui Yu, Jiankun Xiao, Li Gao, Fangfang Gao, Zhuo Kang, Zheng Zhang, Yue Zhang

PII: S2211-2855(19)30033-3
DOI: https://doi.org/10.1016/j.nanoen.2019.01.024
Reference: NANOEN3371

To appear in: *Nano Energy*

Received date: 15 November 2018
Revised date: 25 December 2018
Accepted date: 7 January 2019

Cite this article as: Junli Du, Qingliang Liao, Mengyu Hong, Baishan Liu, Xiankun Zhang, Huihui Yu, Jiankun Xiao, Li Gao, Fangfang Gao, Zhuo Kang, Zheng Zhang and Yue Zhang, Piezotronic Effect on Interfacial Charge Modulation in Mixed-dimensional Van der Waals Heterostructure for Ultrasensitive Flexible Photodetectors, *Nano Energy,* https://doi.org/10.1016/j.nanoen.2019.01.024

Piezotronic Effect on Interfacial Charge Modulation in Mixed-dimensional Van der Waals Heterostructure for Ultrasensitive Flexible Photodetectors

Junli Du[a,1], Qingliang Liao[a,1], Mengyu Hong[a], Baishan Liu[a], Xiankun Zhang[a], Huihui Yu[a], Jiankun Xiao[a], Li Gao[a], Fangfang Gao[a], Zhuo Kang[a], Zheng Zhang[a,b*], Yue Zhang[a,b*]

[a]State Key Laboratory for Advanced Metals and Materials, School of Materials Science and Engineering, University of Science and Technology Beijing, Beijing, 100083, People's Republic of China.

[b]Beijing Key Laboratory for Advanced Energy Materials and Technologies, University of Science and Technology Beijing, Beijing 100083, People's Republic of China.

zhangzheng@ustb.edu.cn

yuezhang@ustb.edu.cn

Abstract

Van der Waals (vdWs) heterostructure is emerging as one of the most interesting systems in next-generation flexible optoelectronics. Furthermore, the gate-tunability of vdWs heterostructure is widely applied to enhance the performance of various devices, which is generally achieved by external electric field. However, in-plane cracking and slippage of gate electrode restricted this external electric field modulation in flexible devices. Here, we propose a distinctive strain-gating method to manipulate 2D WSe_2-1D ZnO vdWs interfacial charge and modulate its photosensing performance by tuning electronic states of WSe_2. With increasing tensile strain, the device shows obvious enhancing photocurrent and the corresponding photoresponsivity reaches up to 394 mA W^{-1} under white light illumination. Such performance enhancement can be attributed to strain-induced piezopolarization charges on ZnO nanobelt polar surface, which function as "gate" to tune the local transport of

[1] These authors contributed equally to this work.

photogenerated carriers at the WSe_2-ZnO vdWs interface. This work provides a new strategy to achieve interaction between vdWs interface and strain stimuli, which broadens applications of functional vdWs heterostructure for next-generation photodetection or imaging.

Graphical abstract

A novel strain-gating strategy is proposed for high-performance mixed-dimensional vdWs flexible photodetector, where strain-induced piezopolarization charges function as "gate" to tune local charge transport process. This work provides an alternative regulation method for carrier manipulation at vdWs heterointerface, which may enable novel structure design for high-performance vdWs optoelectronics.

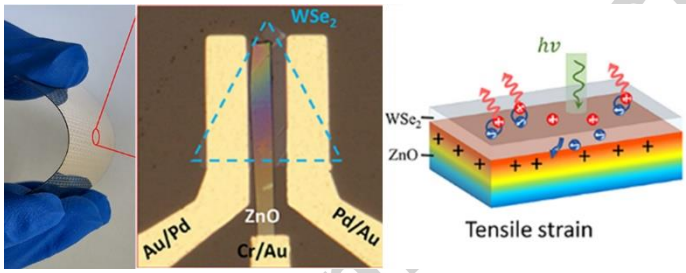

Keywords: Piezotronic effect; Mixed-dimensional vdWs heterostructure; interfacial modulation; self-powered photodetector

1. Introduction

Tuning the property of van der Waals (vdWs) heterostructure by gate has achieved a great deal of application in novel optoelectronics, such as two terminals FET, non-volatile memory, homojunction or heterojunction diodes, photodetector, due to atomic-thickness, unique gate-tunability, excellent mechanical strength, favorable optical and electrical property[1-10]. This gate-tunability is critical to vdWs heterostructure device, which has been achieved by electrostatic gating on hard substrates (e.g., SiO_2/Si) [11-14]. However, it is hard to realize such operation on flexible optoelectronics, as it would introduce extra complexity

during devices fabrication and integration process. Also, in-plane cracking and slippage of gate electrode restricted this external electric field modulation in flexible devices. As is well known, mechanical strain is inevitably generated during the flexible devices bending or stretching process. Therefore, the active interaction between devices and strain is more attractive for flexible electronics/optoelectronics, which means that the device performance could be directly modulated by external mechanical stimuli [15-18]. Using strain-induced piezopotential to gate local charge carrier transport is one of the choices for such requirement [19-26]. In addition, mixed-dimensional vdWs heterostructure can be integrated arbitrarily with materials of different dimensionality, which couple various properties with different dimensional materials to construct high-performance devices [27]. However, the mechanism of this strain-gating interface carrier behavior has not yet been demonstrated for modulating TMDCs based mixed-dimensional heterointerface.

Besides, two-dimensional tungsten diselenide (WSe_2) possesses high carrier mobility up to 350 $cm^2\ V^{-1}\cdot S^{-1}$ and sensational light-matter interactions property [28-32]. The direct bandgap of about 1.67 eV has been observed in monolayer WSe_2. These properties enable it as a good *p*-type semiconductor for constructing *p-n* heterostructure and an excellent candidate for broadband photodetector (PD) [6, 33, 34]. One-dimensional ZnO possess outstanding piezoelectric property and high electron mobility, which can be used to construct high-performance mixed-dimensional vdWs *p-n* heterostructure [20, 29, 35-37]. Here, we have demonstrated a strain-gating method to intensify the photoresponse of WSe_2-ZnO mixed-dimensional vdWs heterostructure flexible PD, which is different from the voltage-gated operation. By applying specific tensile strain, piezopolarization charges are generated at the vicinity of WSe_2-ZnO heterointerface due to the piezoelectric effect. The piezo-charges modulate local charge carrier transport and photogenerated carriers transfer, which ultimately increase the photoresponsivity of devices. Our work indicates a promising structure design for future high-performance flexible devices and a novel regulation strategy for carrier behaviors

manipulation at vdWs heterointerface. Considering that most of the atomic TMDCs are intrinsic piezoelectric, the approach in this work may be extended to other artificial all-2D vdWs structures and inspires the novel structure design for flexible vdWs optoelectronics.

2. Experimental Section

2.1. ZnO nanobelt and layered WSe_2 growth process

ZnO nanobelt was synthesized with chemical vapor deposition method. Silicon wafer deposited with 20 nm thick Au was used as the substrate. The precursor containing mixed ZnO and graphite powder (molar ratio 1:1, 100 mg) was placed in a quartz boat and Au/Si substrate was put face-down above the mixed powder. Prior to heating, the tube was purged with Ar (500 sccm) for 10 min. Then the furnace was heated up to 950 °C with O_2/Ar (3/297 sccm) as the carrier gas, which the synthesis duration was 30 min. For the growth of layered WSe_2, a two-temperature-zone furnace was used. A mixture of $WO_{2.9}$ and KCl (molar ratio 9:1, 10 mg) was loaded in quartz boat at the center of furnace tube (2 inches, zone II) as W source. The Se (40 mg) in the upstream region of the furnace (zone I) served as Se source. The tube furnace was firstly pumped down to ~ 1 Pa to remove air and moisture. Then H_2/Ar (1/20 sccm) carrier gas was introduced until atmospheric pressure was achieved. The W source was heated to 815 °C. Simultaneously, the temperature of Se was increased up to 350 °C. The whole synthesis process was kept for 15 min.

2.2. WSe_2 transfer

A thin layer of poly (methyl methacrylate) (PMMA) was firstly spin-coated on SiO_2/Si substrate with layered WSe_2. The underlying SiO_2 layer was etched away with 1.5% HF solution. Then the detached PMMA/WSe_2 film was lifted from solution and rinsed with DI water. Then, selected WSe_2 nanosheet was transferred onto the ZnO nanobelt with the help of accurate transfer platform (Metatest, E1-T), followed by removing PMMA in hot acetone.

Materials characterization

The crystal structures of ZnO nanobelt and layered WSe_2 were characterized by high-resolution TEM (HRTEM) (FEI Tecnai F20). Their thickness was measured by atomic force microscope (AFM) (Bruker, Dimension Icon). The SKPM of WSe_2-ZnO heterostructure was measured by KPFM measurement (Bruker, Dimension Icon). During the measurement, 1.5 V AC voltage amplitude and 80 Hz frequency were applied to the Pt/Ir tip. The morphology of ZnO nanobelt was observed with field-emission scanning electron microscopy (FESEM) (FEI, Quanta 3D). The Raman, PL spectra measurements were performed on confocal microscopy (Horiba, JY-HR800).

2.3. Device test

The photodetector was excited by a white lamp. The illumination power density was measured by a commercial power meter (THORLABS, PM100D). The strain was applied through a homemade two-point bending apparatus and circular arc approximation was used for computing the applied strain. All of the electrical tests were measured by a semiconducting parameter analyzer (Keithley 4200).

3. Results and discussion

WSe_2-ZnO flexible PD was fabricated by an accurate transfer method, the schematic fabrication process is presented in Figure 1a. Polyethylene terephthalate (PET) was selected as the flexible substrate because of its excellent solvent-resistant and transparent properties. Besides, its relatively high Young's modulus guarantees that bending-induced strain could be effectively transferred to the ZnO nanobelt. The fabrication process started with the transfer of ZnO nanobelt onto PET substrate through PDMS-assisted all-dry transfer method [38]. Here, the length direction of ZnO nanobelt was ensured being parallel to the edge of PET so that bending of substrate induces uniaxial strain in ZnO. Then, the Cr/Au (10 nm/50 nm) electrode was deposited to form an ohmic contact with ZnO. To build mixed-dimensional heterostructure, the layered WSe_2 was subsequently transferred onto the ZnO nanobelt.

Finally, the Pd/Au (10 nm/50 nm) electrode was deposited to form an ohmic contact with WSe_2.

The optical image and operation schematic of the flexible device under tensile strain are shown in Figure 1b and Figure 1c, respectively. The thickness of ZnO nanobelt utilized to construct the device is about 50 nm measured from atomic force microscopy image, as shown in Figure S1a in supporting information. As presented in Figure S1b, high-resolution transmission electron microscopy image and corresponding selected area electron diffraction pattern indicates that synthetic single crystal ZnO nanobelt possesses hexagonal wurtzite structure with growth direction along $[2\bar{1}\bar{1}0]$ and the top polar surface of (0001) [39]. Conventionally, ZnO shows the most significant piezoelectric effect at the surface of (0001), which is beneficial for the interface charge transfer modulation [40-42]. The scanning electron microscopy image and corresponding photoluminescence spectrum of synthetic ZnO nanobelt are shown in Figure S1c, which confirms its high crystallinity.

Figure S1d shows AFM image of WSe_2 nanosheet, indicating its height of 5 nm. The HRTEM image in Figure S1e indicates a good crystalline property of the WSe_2 flake without the presence of grain boundary and dislocations. The Raman spectrum of multi-layer WSe_2 in Figure S1f presents three characteristic peaks of E^1_{2g} (248 cm^{-1}), A_{1g} (259 cm^{-1}) and B_{2g} (307 cm^{-1}) vibration modes, which is consistent with the reported literature [43-45]. The inset image of Figure S1f shows the optical image of layered WSe_2, which exhibits typical triangle morphology with the length about 30 μm.

In order to characterize the heterostructure property and charge transfer among WSe_2-ZnO, the mixed-dimensional vdWs heterostructure on SiO_2/Si substrate was fabricated in accordance with the method shown in Figure 1d. Photoluminescence mapping of the heterostructure is presented in Figure 2a, which depicts an obvious decrease of PL intensity at the WSe_2-ZnO stacked area compared with the as-grown WSe_2 region. Figure 2b shows two typical PL spectra acquired from different points highlighted in Figure 2a inset. Relatively

strong PL intensity around 790 nm can be observed for the layered WSe_2, but the signal drastically declines at WSe_2-ZnO heterostructure. The decrease of PL intensity at stacked area demonstrates that charge transfer exists between WSe_2 and ZnO, as the case observed in other homo- or heterostructures, such as MoS_2 homojunction, MoS_2/WS_2, WS_2/Graphene, MoS_2/WSe_2, MoS_2/Si[46-49]. Due to the existing of the built-in electrical field at the WSe_2-ZnO stacked area, the separation of photogenerated electron-hole pairs in WSe_2 is enhanced, which decreases the measured PL intensity.

To further verify the observed phenomenon and determine specific value of barrier height between WSe_2 and ZnO, SKPM characterization was employed [50]. The contact potential difference (CPD) between AFM tip and the sample is defined as:

$$V_{CPD} = \frac{(\varphi_{tip} - \varphi_{sample})}{q} \quad (1)$$

where φ_{tip}, φ_{sample}, are the work function of tip and sample, q is the elementary charge [46]. As shown in Figure 2c, an obvious surface potential variation exists between WSe_2 and ZnO because of their different Fermi level positions. The CPD data extracted from red line in panel (c) is plotted in Figure 2d, indicating that work function of WSe_2 is 80 meV lower than that of ZnO. Accordingly, the decreased PL intensity and surface potential variation at WSe_2-ZnO heterostructure demonstrate a solid heterojunction contact between layered WSe_2 and ZnO nanobelt.

Schematic sketch of the flexible device is presented in Figure 3a. Typical *I-V* characteristics of WSe_2-ZnO vdWs heterostructure under 0 % strain condition are depicted in Figure 3b, which exhibit obvious rectifying behavior with ON/OFF ratio of 10^4 under ± 1 V applied bias. The reverse leakage current is about 5 fA at -1 V. As shown in Figure S2a-b, typical Ohmic characteristics are observed in Pd-WSe_2 and Cr-ZnO contacts. It can be verified that the rectifying property originates from contact barrier between WSe_2 and ZnO, which is consistent with the PL and SKPM results. In addition, the output characteristics of

WSe_2-ZnO vdWs heterostructure were measured upon illumination with white light from a halogen lamp, which the incident optical power P_{opt} varied from 0.667 to 6.668 $mWcm^{-2}$ and the effective light absorption area of WSe_2-ZnO heterostructure was 45 μm^2. As depicted in Figure 3c, the *I-V* curves shift down under the light illumination, which means an obvious photovoltaic effect in WSe_2-ZnO heterostructure. The photovoltaic phenomenon can be explained by using the schematic band diagram of the vertical stack WSe_2-ZnO heterostructure (Figure 3d). A typical type II band alignment is formed in WSe_2-ZnO heterostructure, in which WSe_2 dominates the light-absorbing because of its smaller bandgap. Considering the carrier concentration of WSe_2 (10^{11}~10^{12} cm^{-2}) [51, 52] and ZnO (10^{16}~10^{18} cm^{-3}) [53], the total *p-n* depletion length is much longer than the p-channel length (~ 5 nm), which results in a monotonic band slope across the entire WSe_2 thickness [12]. Under this built-in electric field, spontaneous separation of photogenerated carriers in WSe_2 gives rise to the photocurrent at 0 V bias.

To precisely characterize the photosensing properties of flexible PD in self-powered mode, the short-circuit current was measured under different illumination. The result is presented in Figure 3e. A simple power law equation is applied to fit the experimental data,

$$I_{photo} \propto P^{\alpha} \quad (2)$$

where I_{photo} is the photocurrent, P is the light illumination intensity, α is the index of a power law (ideal value, α=1). Here, the α value is inferred to be 0.79. The deviation maybe stem from complex processes during the carrier generation, trapping and electron-hole recombination in the semiconductors [54-56]. Another parameter photoresponsivity R of the devices could be calculated from the following formula [57].

$$R = I_{photo}/P \quad (3)$$

As shown in Figure 3f, photoresponsivity has a maximum value of 5 mA W^{-1} and decreases exponentially with the increasing light intensity. This phenomenon can be attributed to inefficient separation of the photogenerated carrier under high illumination.

The PL spectrum of WSe_2-ZnO heterostructure under tensile strain and compressive strain was measured at room temperature to investigate the carrier behaviors manipulation mechanism by piezopolarization charges. Figure S3a, b in the Supporting Information present schematic of the experimental setup and optical image of experimental bending apparatus. Figure S3c exhibits the stimulate area of WSe_2-ZnO heterostructure under compressive strain on the illumination of 532 nm laser. The ZnO nanobelt is placed along the length direction of the PET substrate, while WSe_2 is placed perpendicular to the length direction. This structure garateens that the mainly strain focus on ZnO rather than Wse_2. Figure 4a shows various PL spectrum of the WSe_2-ZnO heterostructure with different compressive and tensile strains. The relationship between PL intensity and strain is exhibited in Figure S4a, indicating an obvious enhancement of PL intensity from tensile strain to compressive strain. Considering the shift and expansion of PL spectrum, it can be deconvoluted with three main components (Figure 4b): the indirect bandgap emission (I), trion exciton (A^-) and the neutral exciton (A). From the extracted PL peak energy in Figure 4b, both peak positions of A^- peak and A peak present an obvious redshift, while the I peak almost maintains a constant value (Figure 4c). Generally, the photoluminescence (PL) intensity of WSe_2 increases and the peak value occurs blueshift under increasing tensile strain according to some relevant literature [58, 59]. This means that the shift of WSe_2 can be attributed to piezopolarization charge rather than the strain-induced lattice deformation, which is similar to the conventional electrostatic-gating result [59].

On the other hand, the trion and neutral exciton PL intensity vary by nearly two times of magnitude from 0.4% compressive strain to 0.4% tensile strain (Figure S4b, Supporting Information). Obvious enhancement of WSe_2 PL intensity is observed under compressive strain, which indicates that the local negative piezopolarization charge inhibits the separation

of photogenerated charge in WSe_2 compared to 0 % strain, as shown in Figure 4d, e. When the heterostructure is stretched, the PL intensity of WSe_2 is suppressed dramatically due to positive piezopolarization charge, which decreases the recombination of photo-induced excitons (Figure 4f). As demonstrated by the above phenomenon, the piezopolarization charges induced by strain can effectively manipulate the local photogenerated charge behavior at the vdWs heterointerface, which is beneficial for the performance modulation of WSe_2-ZnO PD.

From this point, strain-gated WSe_2-ZnO PD photoresponse performance in self-powered mode was investigated by the time-resolved white light response under a defined illumination density of 0.667 mW cm^{-2}. Figure 5a shows the schematic of flexible PD under tensile strain conditions. The time-resolved photoresponse behavior of flexible PD under diverse strain is shown in Figure 5b. An obvious switching behavior is observed, which the current increases rapidly to ON state upon illumination and resumes to OFF state under dark. Besides, it can be seen that the photocurrent increases with increasing tensile strain and decreases with increasing compressive strain. In addition, both the rise and fall time show almost no change under different strain condition, as shown in Figure S5 in the Supporting Information. Furthermore, we extracted the short-circuit current under different strain from Figure 5b and calculated the photoresponsivity (R), as shown in Figure 5c. Both of the I_{SC} and R increase continually as varying from compressive strain to tensile strain. Such monotonous increase indicates that polar piezoelectric effect plays the leading role in this modulation process compared to the piezoresistance effect, which is consistent with the strain-gated PL variation results[60].

To explain this strain-gating mechanism in WSe_2-ZnO PD more clearly, schematic band structures of WSe_2-ZnO interface under tensile and compressive strain upon illumination are shown in Figure 5d, e. The black dotted, red and blue line represents the band structures under 0 %, tensile and compressive strain, respectively. Under tensile strain, as shown in Figure 5d,

positive piezopolarization charges are generated in ZnO nanobelt, which results in a local negative charge carriers accumulation in WSe_2 at the heterointerface, thus further increasing band slope in WSe_2 as the way energy band-modulation with the positive gate voltage. Therefore, the more efficient transport of photogenerated carrier is expected under the extra driving force of such positive piezocharges, which improves the photocurrent of WSe_2-ZnO PD in self-powered mode. On the other hand, negative piezopolarization charges in ZnO are generated when PD suffer from compressive strain, as shown in Figure 5e. This negative charge decreases the band slope of WSe_2 and suppresses the transport of photogenerated carrier in WSe_2, which reduces the overall photoresponse performance.

Another strain-modulated performance of flexible PD in photoconductive mode was investigated under light illumination at 1V applied bias. This operation mode can achieve high photoresponsivity in a flexible device with the synergistic effect of piezo-phototronic. Figure 6a shows the *I-V* curve in defined light illumination of 0.667 mW cm^{-2} under different strain. We extracted the photocurrent at 1 V applied bias with various light illumination under different strain, which is shown in Figure 6b. The current was enhanced by 6.3 times under 0.87% tensile strain compared to 0 % strain condition. To demonstrate photoresponse performance clearly, *R* under a certain external strain is calculated and listed in Figure 6c. As external tensile strains increase, the value of *R* increases gradually under same light illumination with the maximum values of 394 mA W^{-1}. The photogain is calculated from the following formula

$$Gain = h\vartheta I_{ph}/Pe, \quad (4)$$

where h is Plank's constant; ϑ and P is the frequency and intensity of the incident light; I_{ph} is the photocurrent; e is the unit charge, respectively. $Gain/Gain_0$ is defined as the relative ratio under certain strain and 0 % strain. The relative ratio of photogain exhibits the same increasing trend as *R* under different strain on a defined light illumination in Figure 6d.

However, detectivity of devices exhibits an slight decline with increasing strain under a defined light intensity of 2.32 mW cm^{-2} and 5.21 mW cm^{-2}, as shown in Figure 6e.

$$D^* = R_i/(2e \cdot I_{dark}/A)^{1/2} \quad (5)$$

According to the formula, the detectivity is inversely proportional to dark current[61]. The dark current ascends from compressive strain to tensile strain in the strain-modulated device (Figure S6, Supporting Information), which result in the decrement of detectivity. In addition, photoresponse performance figure-of-merits of flexible PD are summarized in Table S1. Obviously, our devices exhibit excellent photoresponsivity, which indicates that this strain-gating method can effectively optimize the performance of devices.

4. Conclusion

In conclusion, a strain-gating strategy has been achieved by using piezotronic effect for high performance WSe_2-ZnO flexible photodetector. We systematically proposed and demonstrated the strain-gating mechanism, in which the stain-induced piezopolarization charges effectively regulate the charge transport at WSe_2-ZnO vdWs heterointerface. With increasing tensile strain, the performance of photodetector in self-powered mode exhibits an obvious enhancement of response current and photoresponsivity. While in photoconductive mode, the device presents an enhanced photocurrent from 61 pA to 320 pA and photoresponsivity increases from 117 mA W^{-1} to 394 mA W^{-1}. Our work provides a promising strain-engineered strategy to modulate vdWs heterointerface and paves a way for next-generation flexible optoelectronics.

Acknowledgments

This work was supported by the National Natural Science Foundation of China (No. 51527802, 51602020, 51722203, and 51672026), Overseas Expertise Introduction Projects for Discipline Innovation (No. B14003), National Key Research and Development Program of China (No. 2016YFA0202701), Beijing Municipal Science & Technology Commission

(Z161100002116027), the Fundamental Research Funds for the Central Universities (FRF-TP-18-001C1, FRF-BD-18-012A). Junli Du and Qingliang Liao contributed equally to this work.

Competing financial interests

The authors declare no competing financial interests.

Appendix A. Supporting information

The supporting information is available free of charge on the Publications website. Supplementary methods, and additional experimental data (Figs. S1–S5, Table S1).

References

[1] K.L. Seyler, J.R. Schaibley, P. Gong, P. Rivera, A.M. Jones, S. Wu, J. Yan, D.G. Mandrus, W. Yao, X. Xu, Nat. Nanotechnol. 10 (2015) 407-411.

[2] P. Lin, C. Pan, Z. Wang, Mater. Today Nano, accepted.

[3] Y. Wang, J. Xiao, H. Zhu, Y. Li, Y. Alsaid, K.Y. Fong, Y. Zhou, S. Wang, W. Shi, Y. Wang, A. Zettl, E.J. Reed, X. Zhang, Nature 550 (2017) 487-491.

[4] J. Shim, J.K. Kim, K.S. Lee, C.-L Lee, M. Ma, W.K. Choi, J.Y. Hwang, H. Yang, B. Angadi, J.Y. Park, K. Yu, D. Son, Nano Energy 25 (2016) 9-17.

[5] D. Costanzo, S. Jo, H. Berger, A.F. Morpurgo, Nat. Nanotechnol. 11 (2016) 339-344.

[6] R. Bao, Y. Hu, Q. Yang, C. Pan, MRS Bull. 43 (2018) 952-958.

[7] G. Cao, A. Shang, C. Zhang, Y. Gong, S. Li, Q. Bao, X. Li, Nano Energy 30 (2016) 260-266.

[8] X. Liu, R. Liang, G. Gao, C. Pan, Q. Xu, C. Jiang, J. Luo, X. Zou, Z.Y. Yang, L. Liao, Z. Wang, Adv. Mater. (2018) 1800932.

[9] Y. Xiao, L. Fu, Sci. China Mater. 61 (2017) 761-762.

[10] J. Liu, H. Cao, B. Jiang, Y. Xue, L. Fu, Sci. China Mater. 59 (2016) 459-474.

[11] B.W.H. Baugher, H.O.H. Churchill, Y. Yang, P. Jarillo-Herrero, Nat. Nanotechnol. 9 (2014) 262-267.

[12] W. Yu, Y. Liu, H. Zhou, A. Yin, Z. Li, Y. Huang, X. Duan, Nat. Nanotechnol. 8 (2013) 952-958.

[13] D. Jariwala, V.K. Sangwan, C. Wu, P. Prabhumirashi, M.L. Geier, T.J. Marks, L.J. Lauhon, M.C. Hersam, Proc. Natl. Acad. Sci. U. S. A. 110 (2013) 18076-18080.

[14] Z. Yang, L. Liao, F. Gong, F. Wang, Z. Wang, X. Liu, X. Xiao, W. Hu, J. He, X. Duan, Nano Energy 49 (2018) 103-108.

[15] T. Shen, A.V. Penumatcha, J. Appenzeller, ACS Nano 10 (2016) 4712-4718.

[16] P. Lin, L. Zhu, D. Li, L. Xu, C. Pan, Z. Wang, Adv. Funct. Mater. 28 (2018) 1802849.

[17] G. Hu, W. Guo, R. Yu, X. Yang, R. Zhou, C. Pan, Z. Wang, Nano Energy 23 (2016) 27-33.

[18] G Zhang, Q. Liao, M. Ma, F. Gao, Z. Zhang, Z. Kang, Y. Zhang, Nano Energy 52 (2018) 501-509.

[19] Y. Zhang, X.Q. Yan, Y. Yang, Y. Huang, Q. Liao, J. Qi, Adv. Mater. 24 (2012) 4647-4655.

[20] Y. Zhang, Y. Yang, Y. Gu, X. Yan, Q. Liao, P. Li, Z. Zhang, Z. Wang, Nano Energy 14 (2015) 30-48.

[21] W. Wu, X. Wen, Z. Wang, Science 340 (2013) 952-957.

[22] Y. Zhang, W. Jie, P. Chen, W. Liu, J. Hao, Adv. Mater. 30 (2018) 1707007.

[23] M.-CWong, L. Chen, G. Bai, L.-B Huang, J. Hao, Adv. Mater. 29 (2017) 1701945.

[24] M.-C Wong, L. Chen, M.-K Tsang, Y. Zhang, J. Hao, Adv. Mater. 27 (2015) 4488-4495.

[25] Z. Pan, W. Peng, F. Li, Y. He, Nano Energy 49 (2018) 529-537.

[26] S. Qiao, J. Liu, G. Fu, K. Ren, Z. Li, S. Wang, C.F. Pan, Nano Energy 49 (2018) 508-514.

[27] D. Jariwala, T. Marks, M.C. Hersam, Nat. Mater. 16 (2016) 170-181.

[28] X. Hong, J. Kim, S.-F. Shi, Y. Zhang, C. Jin, Y. Sun, S. Tongay, J. Wu, Y. Zhang, F. Wang, Nat. Nanotechnol. 9 (2014) 682-686.

[29] M.H. Chiu, M. Li, W. Zhang, W.T. Hsu, W. Chang, M. Terrones, H. Terrones, L. Li, ACS Nano 8 (2014) 9649-9656.

[30] X. Wen, W. Xu, W. Zhao, J.B. Khurgin, Q. Xiong, Nano Lett. 18 (2018) 1686-1692.

[31] A. Avsar, K. Marinov, E.G. Marin, G. Iannaccone, K. Watanabe, T. Taniguchi, G. Fiori, A. Kis, Adv. Mater. 30 (2018) e1707200.

[32] L.Ye, P. Wang, W. Luo, F. Gong, L. Liao, T. Liu, L. Tong, J. Zang, J. Xu, W. Hu, Nano Energy 37 (2017) 53-60.

[33] S.-H. Jo, D.-H. Kang, J. Shim, J. Jeon, M.H. Jeon, G. Yoo, J. Kim, J. Lee, G.Y. Yeom, S. Lee, H.-Y. Yu, C. Choi, J.-H. Park, Adv. Mater. 28 (2016) 4824-4831.

[34] M.M. Furchi, A. Pospischil, F. Libisch, J. Burgdörfer, T. Mueller, Nano Lett. 14 (2014) 4785-4791.

[35] P. Li, Q. Liao, S. Yang, X. Bai, Y. Huang, X. Yan, Z. Zhang, S. Liu, P. Lin, Z. Kang, Y. Zhang, Nano Lett. 14 (2014) 480-485.

[36] Z. Zhang, J. Du, B. Li, S. Zhang, M. Hong, X. Zhang, Q. Liao, Y. Zhang, APL Mater. 5 (2017) 086111.

[37] S. Liu, Q. Liao, S. Lu, Z. Zhang, G. Zhang, Y. Zhang, Adv. Funct. Mater. 26 (2016) 1347-1353.

[38] P. Lin, L. Zhu, D. Li, L. Xu, Z. Wang, Nanoscale 10 (2018) 14472-14479.

[39] P. Lin, X. Yan, Z. Zhang, Y. Shen, Y. Zhao, Z. Bai, Y. Zhang, ACS Appl. Mater. Interfaces 5 (2013) 3671-3676.

[40] Z. Zhang, Q. Liao, X. Zhang, G. Zhang, P. Li, S. Lu, S. Liu, Y. Zhang, Nanoscale 7 (2015) 1796-1801.

[41] S. Liu, Q. Liao, Z. Zhang, X. Zhang, S. Lu, L. Zhou, M. Hong, Z. Kang, Y. Zhang, Nano Res. 10 (2017) 3476-3485.

[42] P. Ghamgosar, F. Rigonia, S.J. You, I. Dobryden, M.G. Kohan, A.L. Pellegrino, I. Concina, N. Almqvist, G. Malandrinoc, A. Vomiero, Nano Energy 51 (2018) 308–316.

[43] M. Chen, B. Z, G. Hu, X. Fang, H. Wang, L. Wang, J. Luo, X. Han, X. Wang, C. Pan, Z. Wang, Adv. Funct. Mater. (2018) 1706379.

[44] T. Yamaoka, H.E. Lim, S. Koirala, X. Wang, K. Shinokita, M. Maruyama, S. Okada, Y. Miyauchi, K. Matsuda, Adv. Funct. Mater. 28 (2018) 1801021.

[45] H. Zhou, C. Wang, J.C. Shaw, R. Cheng, Y. Chen, X.Q. Huang, Y. Liu, N.O. Weiss, Z.Y. Lin, Y. Huang, X.F. Duan, Nano Lett. 15 (2014) 709-713.

[46] X. Zhang, Q. Liao, S. Liu, Z. Kang, Z. Zhang, J. Du, F. Li, S. Zhang, J. Xiao, B. Liu, Y. Ou, X. Liu, L. Gu, Y. Zhang, Nat. Commun. 8 (2017) 15881.

[47] W. Wu, Q. Zhang, X. Zhou, L. Li, J. Su, F. Wang, T. Zhai, Nano Energy 51 (2018) 45-53.

[48] Y. Xue, Y. Zhang, Y. Liu, H. Liu, J. Song, J. Sophia, J. Liu, Z. Xu, Q. Xu, Z. Wang, J. Zheng, Y. Liu, S. Li, Q. Bao, ACS Nano 10 (2015) 573-580.

[49] L. Britnell, R.M. Ribeiro, A. Eckmann, R. Jalil, B.D. Belle, A. Mishchenko, Y.J. Kim, R.V. Gorbachev, T. Georgiou, S.V. Morozov, A.N. Grigorenko, A.K. Geim, C. Casiraghi, A.H.C. Neto, K.S. Novoselov, Science 340 (2013) 1311-1314.

[50] S. Qiao, R. Cong, J. Liu, B. Liang, G. Fu, S. Wang,W. Yu, K. Ren, C. Pan, J. Mater. Chem. C 6 (2018) 3233-3239.

[51] Z. Wang, Y. Gu, J. Qi, S. Lu, P. Li, P. Lin, Y. Zhang, RSC Adv. 5 (2015) 42075-42080.

[52] A. Allain, A. Kis, ACS Nano 8 (2014) 7180-7185.

[53] J.I. Wang, Y. Yang, Y.A. Chen, K. Watanabe, T. Taniguchi, H.O. Churchill, P. Jarillo-Herrero, Nano Lett. 15 (2015) 1898-1903.

[54] B. Ehrler, K.P. Musselman, M.L. Bohm, F.S. Morgenstern, Y. Vaynzof, B.J. Walker, J.L. Macmanus-Driscoll, N.C. Greenham, ACS Nano, 7 (2013) 4210-4220.

[55] H. Kind, H. Yan, B. Messer, M. Law, P. Yang, Adv. Mater. 14 (2002) 158-160.

[56] X. Liu, L. Gu, Q. Zhang, J. Wu, Y. Long, Z. Fan, Nat. Commun. 5 (2014) 4007.

[57] F. Wang, Z. Wang, L. Yin, R. Cheng, J. Wang, Y. Wen, T.A. Shifa, F. Wang, Y. Zhang, X. Zhan, J. He, Chem. Soc. Rev. 47 (2018) 6296-6341.

[58] Y. He, Y. Yang, Z. Zhang, Y. Gong, W. Zhou, Z. Hu, G. Ye, X. Zhang, E. Bianco, S. Lei, Z. Jin, X. Zou, Y. Yang, Y. Zhang, E. Xie, J. Lou, B. Yakobson, R. Vajtai, B. Li, P. Ajayan, Nano Lett. 16 (2016) 3314-3320.

[59] S.B. Desai, G. Seol, J.S. Kang, H. Fang, C. Battaglia, R. Kapadia, J.W. Ager, J. Guo, A. Javey, Nano Lett. 14 (2014) 4592-4597.

[60] Q.H. Wang, K. Kalantar-Zadeh, A. Kis, J.N. Coleman, M.S. Strano, Nat. Nanotechnol., 7 (2012) 699-712.

[61] N. Huo, G. Konstantatos, Adv. Mater. (2018) e1801164.

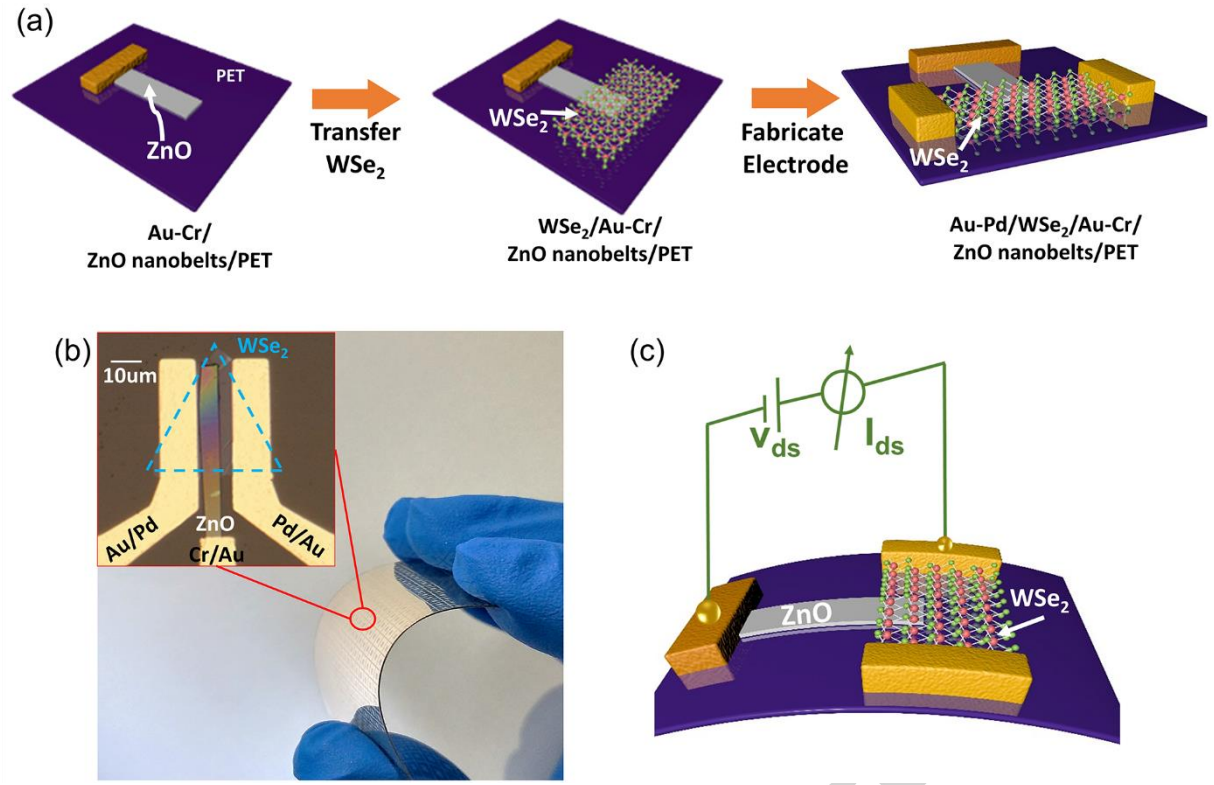

Figure 1. (a) Schematic fabrication process of flexible p-n photodetector with few-layer WSe_2-ZnO nanobelt. (b) Optical image of the flexible photodetector under tensile strain. Inset: a flexible photodetector with few-layer WSe_2, ZnO nanobelts and electrodes. (c) Operation schematic of flexible p-n photodetector with few-layer WSe_2-ZnO nanobelt.

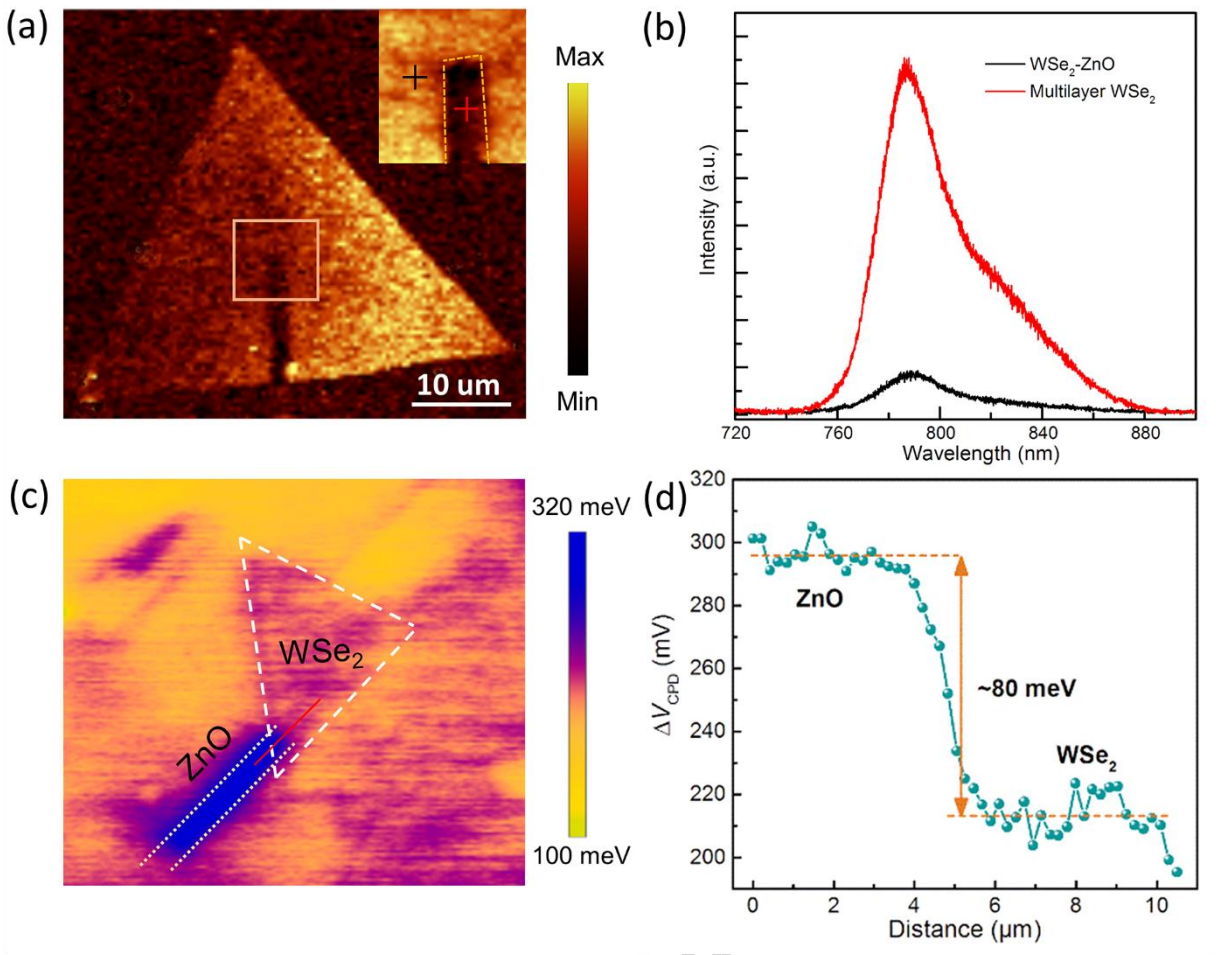

Figure 2. PL mapping and SKPM characterization of WSe_2-ZnO vdWs heterostructure. (a) PL mapping of the WSe_2-ZnO vdWs heterostructure. Inset: partial enlargement of PL mapping in orange rectangle area, PL mapping of WSe_2-ZnO stack area in orange dash line. (b) PL spectrum acquired from different points highlighted in (a) inset. (c) SKPM images of WSe_2/ZnO junction area. The white dash line area represents WSe_2 and white point dash line area represents ZnO. (d) CPD value between layered WSe_2 and ZnO nanobelt with the data extracted from red line in **c** the value is about 80 meV.

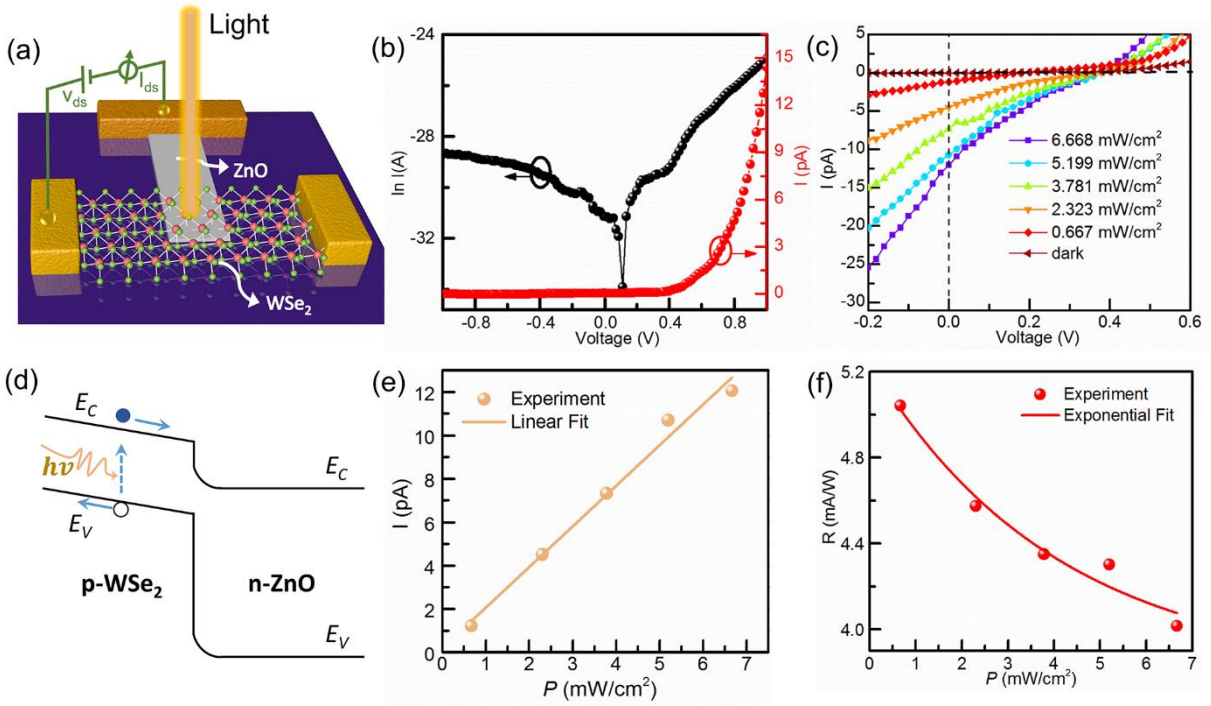

Figure 3. Electrical and photoresponse properties of WSe_2-ZnO vdWs heterostructure. (a) Schematic diagram of WSe_2-ZnO PD on flexible PET substrate. (b) Current-voltage curves of the flexible WSe_2-ZnO diode in linear and logarithmic scale under 0 % strain. (c) *I-V* characteristics of the WSe_2-ZnO PD with different optical illumination intensity under 0 % strain. (d) Schematic illustration of photovoltaic effect in WSe_2-ZnO heterostructure. The blue arrow represents the electrons/holes moving direction. (e) Photocurrent and responsivity f) as a function of illumination intensity of the WSe_2-ZnO PD.

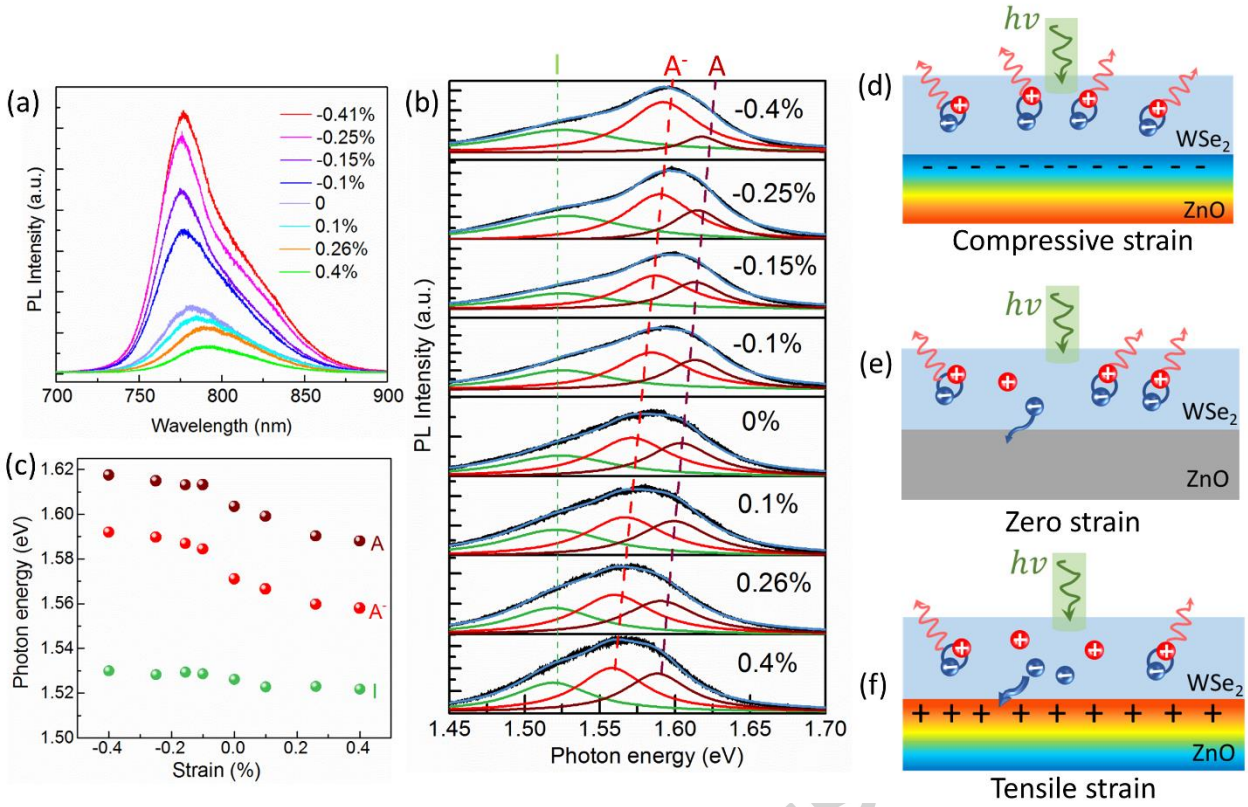

Figure 4. Photoluminescence property of WSe_2-ZnO heterostrucuture under different strain. (a) photoluminescence spectra of WSe_2 under different strain condition. The positve and negative percentage represent tensile and compressive strains, respectively. (b) photoluminescence spectra (dark lines) in the range of 1.45-1.7 eV for the indicated strain. The indirect band gap emission (I), neutral exciton (A) and trion (A^-) resonances behave differently with strain. The blue line is lorenzian fits to the experimental results, with the I, A^- and A components shown as the green, red, claret lines, respectively. (c) photon energy of I, A^- and A, determined from the PL spectra, as a function of strain. (d) Schematic of photogenerated charge modulated by compressive strain, (e) modulated by 0 % strain, f) modulated by tensile strain, respectively.

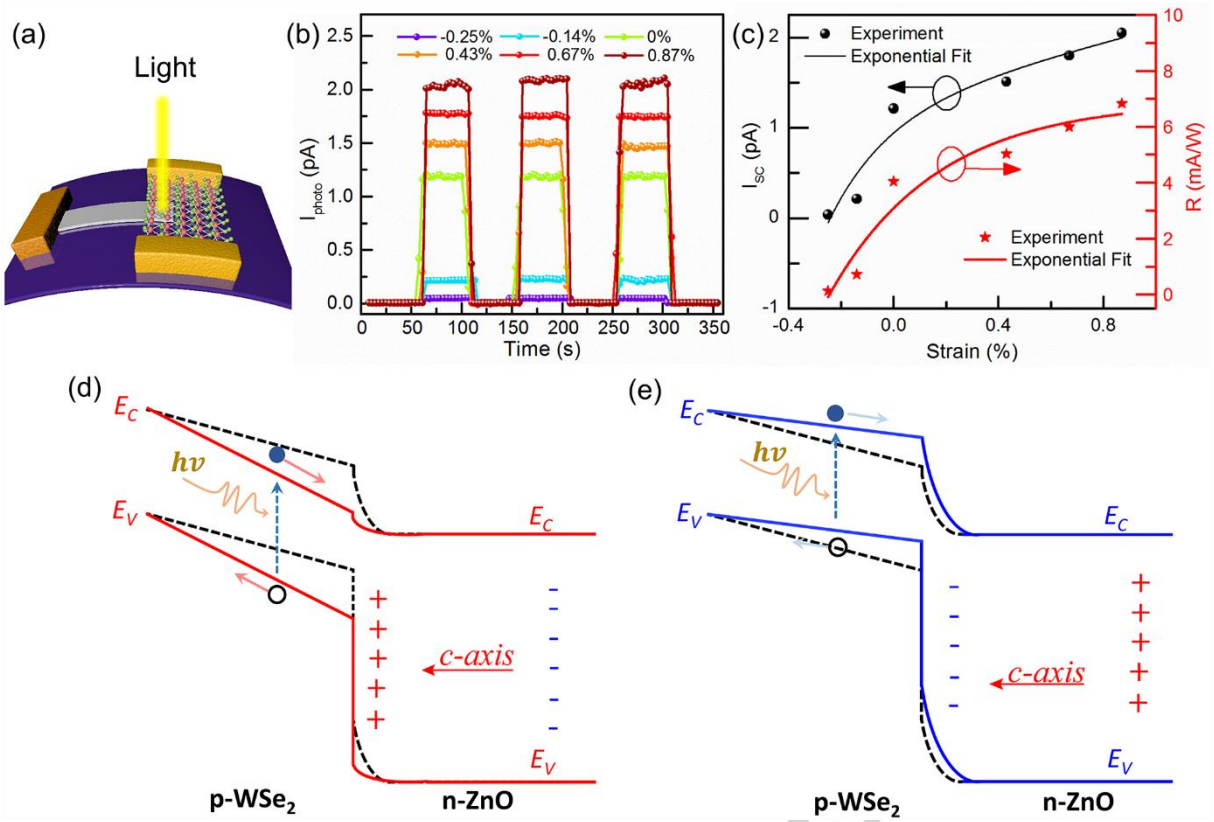

Figure 5. Piezoelectric-gated performance of self-powered WSe_2-ZnO PD. (a) Schematic of flexible WSe_2-ZnO PD under tensile strain at light illumination. (b) Time-resolved photoresponse of the WSe_2-ZnO vdWs PD under different strain and fixed illumination density of 0.667 mW cm^{-2} at 0 V bias. (c) Strain dependence of short-circuit current I_{SC} and R of the flexible WSe_2-ZnO PD. (d) Schematic energy-band diagrams modulation of WSe_2-ZnO heterostructure under tensile strain and (e) compressive strain. Holes, electrons, photons, positive piezopolarization charges, negative piezopolarization charges are represented by blue dots, black circles, orange arrows, red mark "+" and blue mark "-", respectively. The black dotted line represents initial band slope. The red line in (d) represents band structure under tensile strain, while blue line in (e) represents band structure under compressive strain.

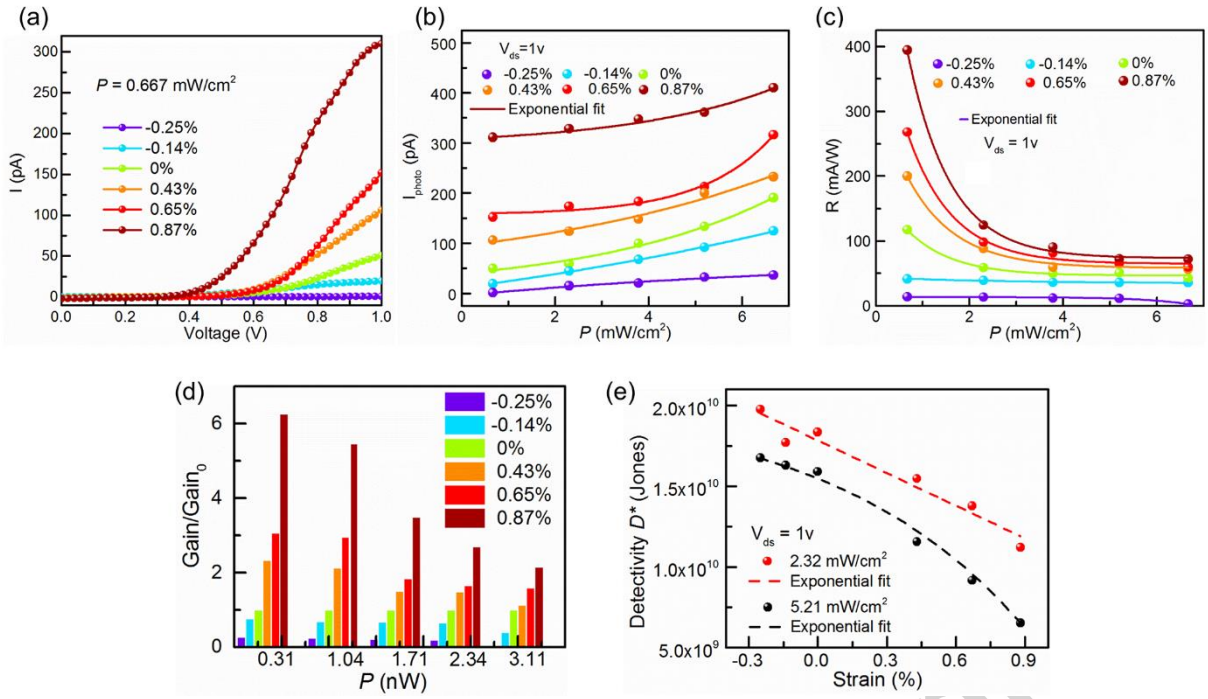

Figure 6. Piezoelectric-gated performance of WSe_2/ZnO PD in photoconductive mode. (a) Typical output characterization of the WSe_2-ZnO heterojunction under various strain and fixed illumination density of 0.667 $mWcm^{-2}$. (b) Strain-dependent photocurrent, (c) responsivity and (d) relative photogain of the device for different illumination intensity under 1V applied external bias. (e) Strain-dependent detectivity under defined illumination intensity of 2.32 mW cm^{-2} and 5.21 mW cm^{-2}.

Vitae

Junli Du received her B.S. from Guangxi University (China) in 2014. She is now a Ph.D student under the guidance of Prof. Yue Zhang at School of Materials Science and Engineering, University of Science and Technology Beijing. Her research focuses on performance modulation with multi-field coupling effect in 2D layered materials and vdWs heterostructures.

Qingliang Liao received his Ph.D. degree from University of Science and Technology Beijing (USTB) in 2009. Now he is a professor at School of materials science and Engineering in USTB. His scientific interests focus on synthesis and characterization of one-dimensional nanomaterials, design and application of functional nanodevices.

Mengyu Hong received her B.S. degree from University of Science and Technology Beijing in 2016. Now, she is a Ph.D. student in the school of University of Science and Technology Beijing. Her research focus on fabrication and characterization of 2D material based photodetectors.

Baishan Liu revived his B.E. degree from University of Science and Technology Beijing in 2015. Now he is a Ph. D candidate at School of Materials Science and Engineering in University Technology Beijing. His research interests focus on strain engineering on 2D materials.

Xiankun Zhang received her B.S. degree in School of Sciences from Hubei University in 2014. He is currently under the supervision of Prof. Yue Zhang at

the School of Materials Science and Engineering in University of Science and Technology Beijing. His research interests focus on 2D materials based defect engineering, photoelectrical nanodevices, and electronic devices.

Huihui Yu received her B.E. degree from Inner Mongol University of Technology in 2016. Now she is a Ph.D candidate at School of Materials Science and Engineering in University of Science and Technology Beijing. Her research interests focus on high performance photodetectors in 2D materials.

Jiaokun Xiao received his B.E. degree from University of Jinan in 2012. Now he is a Ph.D candidate at School of Materials Science and Engineering in

University of Science and Technology Beijing. His research interests focus on high performance electronic devices in 2D materials.

Zhuo Kang received his Ph.D. degree from University of Science and Technology Beijing (USTB) in 2016. Now he is a lecturer at School of materials science and Engineering in USTB. His research interests focus on ZnO based photoelectric nanodevice, photoelec-trochemical cell and solar cell.

Zheng Zhang received his Ph.D. degree from University of Science and Technology Beijing (USTB) in 2015. Now he is an associate professor at School of materials science and Engineering in USTB. His research interests focus on low dimensional nanomaterials such as 1D ZnO and 2D TMDCs and their heterostructure for optical applications.

Yue Zhang is a professor of material physics in University of Science and Technology Beijing, China. He has been awarded the financial support for outstanding young scientist foundation of China and selected as the chief scientist of Major National Scientific Research Projects. His research focuses on functional nano-materials and nano-devices, new energy materials, and nanoscale failure and service behavior. He has published more than 350 papers in peer reviewed scientific journals and 8 monograph, and held 25 patents in his research area. His publication has been cited more than 10000 times by peers.

Highlights

- Mixed-dimensional vdWs flexible photodetector is constructed with 2D WSe_2 and 1D ZnO nanobelt.
- WSe_2-ZnO interface charge state and hence the photodetection performance is effectively modulated with strain-induced piezopolarization charges.
- The modulation impact of piezotronic effect is verified with photoluminescence characterization.
- The response current and photoresponsivity exhibit 2 times enhancement in self-powered mode under modulation of piezotronic effect.